Resonant Ultrasound Spectroscopy for Irregularly Shaped Samples and Its Application to Uranium Ditelluride

Florian Theuss,[1] Gregorio de la Fuente Simarro,[1] Avi Shragai,[1] Gael Grissonnanche,[1] Ian M. Hayes,[2] Shanta Saha,[2] Tatsuya Shishidou,[3] Taishi Chen,[4] Satoru Nakatsuji,[4,5,6,7] Sheng Ran,[8] Michael Weinert,[3] Nicholas P. Butch,[2,9] Johnpierre Paglione,[2,10] and B. J. Ramshaw[1,10,*]

[1]*Laboratory of Atomic and Solid State Physics, Cornell University, Ithaca, New York 14853, USA*
[2]*Quantum Materials Center, Department of Physics, University of Maryland, College Park, Maryland 20742, USA*
[3]*Department of Physics, University of Wisconsin-Milwaukee, Milwaukee, Wisconsin 53201, USA*
[4]*The Institute for Solid State Physics, The University of Tokyo, Kashiwa, Chiba 277-8581, Japan*
[5]*Department of Physics, The University of Tokyo, Tokyo 113-0033, Japan*
[6]*Institute for Quantum Matter and Department of Physics and Astronomy, Johns Hopkins University, Baltimore, Maryland 21218, USA*
[7]*Trans-scale Quantum Science Institute, University of Tokyo, Tokyo 113-0033, Japan*
[8]*Department of Physics, Washington University in St. Louis, St. Louis, Missouri 63130, USA*
[9]*NIST Center for Neutron Research, National Institute of Standards and Technology, 100 Bureau Drive, Gaithersburg, Maryland 20899, USA*
[10]*Canadian Institute for Advanced Research, Toronto, Ontario, Canada*

(Received 16 March 2023; revised 22 August 2023; accepted 11 January 2024; published 9 February 2024; corrected 19 March 2024)

Resonant ultrasound spectroscopy (RUS) is a powerful technique for measuring the full elastic tensor of a given material in a single experiment. Previously, this technique was practically limited to regularly shaped samples such as rectangular parallelepipeds, spheres, and cylinders [W. M. Visscher *et al.* J. Acoust. Soc. Am. **90**, 2154 (1991)]. We demonstrate a new method for determining the elastic moduli of irregularly shaped samples, extending the applicability of RUS to a much larger set of materials. We apply this new approach to the recently discovered unconventional superconductor UTe_2 and provide its elastic tensor at both 300 and 4 kelvin.

DOI: 10.1103/PhysRevLett.132.066003

Introduction.—UTe_2 is a recently discovered unconventional superconductor [1] with upper critical fields as high as 65 tesla compared to a critical temperature that is at most 2 kelvin [1–3], and an nuclear magnetic resonance Knight shift [4–6] that suggest spin-triplet pairing. There are, however, many unsolved mysteries in UTe_2, including field-reentrant superconductivity [7–10], time-reversal symmetry breaking [11,12], a phase transition between superconducting ground states as a function of magnetic field [13], and the occurrence of two superconducting transitions in certain samples [12,14–16].

Externally applied stress has proven to be a useful tuning parameter when investigating these types of questions. For example, there are two unambiguous superconducting phase transitions in UTe_2 under hydrostatic pressure [10,17], and uniaxial pressure experiments [18] imply an insensitivity of the superconducting order parameter to shear strain. However, while stress and pressure are conceptually straightforward parameters to tune externally, the more physically relevant quantity—related to microscopic bond distances and unit cell volumes—is strain. Stress, σ, and strain, ε, are linearly related through the elastic tensor, $\sigma = \boldsymbol{c}\varepsilon$, and converting from the experimentally applied stress to strain requires the full elastic tensor. For example, the full elastic tensor was central in determining the quantitative relationship between strain, the van Hove point, and superconductivity in Sr_2RuO_4 [19,20], as well as the relationship between anisotropic strains and superconductivity in $CeIrIn_5$ [21].

The full elastic tensor of a material can be determined with resonant ultrasound spectroscopy (RUS). RUS measures the mechanical resonance spectrum of a three-dimensional solid. The resonance frequencies are determined by both intrinsic sample properties—the density and elastic moduli—as well as by the sample boundary conditions. If the elastic moduli, density, and sample geometry are known, then the resonance frequencies are easily calculated numerically—the "forward problem"—either using the method of Visscher *et al.* [22] or by finite elements [23,24]. The inverse problem—obtaining the elastic moduli from a measured resonance spectrum—is more challenging because it requires multiple numerical evaluations of the forward problem and the navigation of a complex parameter landscape with many local minima [25].

For simple geometries with easily defined boundaries—typically rectangular parallelepipeds, cylinders, or spheres—the method of Visscher *et al.* [22] can be combined with either Levenberg-Marquardt or heuristic (such as genetic algorithm) fitting methods to solve the inverse problem and

obtain the elastic moduli from the resonance spectrum. For irregular samples, however, finite elements has been traditionally used to solve the forward problem [23,24]. The difficulty with this approach is that finite elements is too computationally intensive to use when solving the inverse problem. This has largely restricted the applicability of RUS to materials where regularly shaped samples can be prepared.

In the case of UTe_2, preparation of a rectangular parallelepiped is difficult due to the brittle nature of the material (in addition to the potential hazards associated with polishing uranium compounds). In this Letter, we take advantage of the recent development by Shragai *et al.* [26] that solves the forward problem for irregularly shaped samples in a way that is two orders of magnitude faster than finite elements. This has allowed us to develop a protocol for solving the inverse problem for irregularly shaped samples. We demonstrate this protocol on single-crystal samples of $SrTiO_3$ and Mn_3Ge—compounds with known elastic moduli—and then apply our new technique to obtain the full elastic tensor of UTe_2 at 300 K and at 4 K.

Methods: Resonant ultrasound spectroscopy.—We performed RUS measurements by placing a sample in weak mechanical contact between two piezoelectric transducers, providing nearly free boundary conditions. One transducer is driven with an ac voltage at fixed frequency, and the voltage generated on the other transducer is measured using a lockin amplifier. By stepping the drive frequency from roughly 100 kHz to 5 MHz, we obtain the first 100 or so mechanical resonances for a typical, mm-scale sample. More details of the experimental setup and how to measure resonance spectra can be found in Ramshaw *et al.* [25] and Balakirev *et al.* [27]. Full lists of all experimental resonance spectra used in this Letter are given in the Supplemental Material (SM) [28].

Methods: Fitting resonance spectra.—Resonance spectra are calculated by minimizing the linear elastic Lagrangian as a function of the displacement field $\vec{u}(\vec{r},t)$,

$$\mathcal{L} = \frac{1}{2}\int \left(\sum_i \rho \dot{u}_i^2(\vec{r}) - \sum_{ijkl} c_{ijkl} \frac{\partial u_i(\vec{r})}{\partial r_j} \frac{\partial u_k(\vec{r})}{\partial r_l} \right) dV, \qquad (1)$$

where ρ is the density, c_{ijkl} is the elastic tensor, and the integral is over the entire volume of the sample. The widely adopted method of Visscher *et al.* [22] expands the displacements fields in a polynomial basis and solves the volume integrals analytically. This method only works for rectangular parallelepipeds, cylinders, spheres, or other regular shapes with analytically defined boundaries [22,27]. For irregularly shaped samples, however, this method is insufficient and new methods for computing the resonance spectra must be used.

We implement two resonance spectra calculation methods—two "forward" solvers—into a genetic algorithm, extending the RUS fitting routine to irregularly shaped samples. Details of the genetic algorithm itself can be found in Ramshaw *et al.* [25] and in the SM [28]; here we focus on incorporating and verifying the new forward solvers to obtain the elastic moduli of UTe_2.

The first forward solver extends Visscher's method to irregular samples [26]. The displacement fields in Eq. (1) are expanded in the same polynomial basis as in Visscher *et al.* [22]. Instead of evaluating the integrals over the volume of the sample, however, we use Gauss's law to project the integrals onto the surface of the sample. This allows us to evaluate the integrals for arbitrary shapes as long as the surface is encoded by a mesh of triangles. We will refer to fits performed with this forward solver as SMI (surface mesh integration [26]).

The second forward solver is a commercially available finite element solver: Comsol. We implement a Comsol forward solver to verify the use of the newer SMI method when fitting elastic moduli (i.e. when solving the inverse problem: the use of FEM to calculate the forward problem for RUS was described earlier in Liu and Maynard [23]). We will refer to fits performed using Comsol as the forward solver as FEM.

Both SMI- and FEM-based fits are compared to fits using Visscher's approach for rectangular parallelepiped samples. Fits with Visscher's approach are referred to as RPR. To facilitate comparison between the different methods, we fix the number of resonances to 70 (84) for all $SrTiO_3$ (Mn_3Ge) fits, and we expand the displacement field to 18^{th} order for both the RPR and SMI methods (FEM does not expand the displacements in a polynomial basis).

Methods: Sample digitization and alignment.—Both the SMI and FEM methods require three-dimensional digitizations of the samples. FEM uses the full, three-dimensional tetrahedral mesh of the entire sample volume. SMI uses only the surface triangles of the same mesh (this includes any "interior" surfaces around voids). These digitizations were obtained with a Zeiss Xradia Versa XRM-520 X-ray nano-CT and are shown in Fig. 1. The mesh size used for our fits depends on the solver method, as well as on the sample shape and size. We use a mesh with average linear dimension 10 μm for SMI, and 60 μm for FEM (FEM uses a larger mesh because it is much more computationally intensive than SMI). The samples are oriented to within

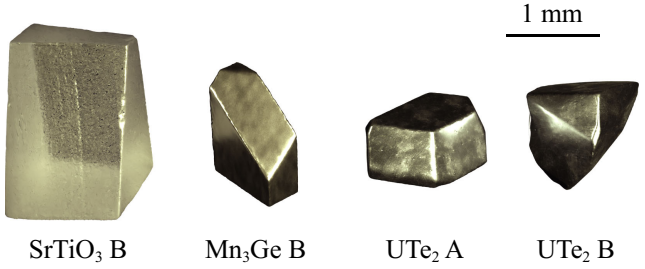

FIG. 1. CT scan models. 3D models of the irregularly shaped samples used for RUS measurements based on CT scans. From left to right: $SrTiO_3$ sample B, Mn_3Ge sample B, UTe_2 sample A, UTe_2 sample B.

1 degree using Laue backreflection diffractometry. The mesh is then aligned to the crystal axes by identifying two flat faces on the sample which uniquely relate the surface mesh to the orientation of the sample in the Laue apparatus. More details on sample digitization can be found in the SM [28].

Methods: Measurement uncertainty.—The quality of each fit is characterized by the root mean square (rms) of the difference between experimentally measured and calculated resonances. The uncertainties in the elastic moduli are estimated by calculating the change in elastic modulus needed to produce a 2% increase of the rms error [27,29].

We further identify three dominant systematic errors: (i) deviations from the weak-coupling approximation due to the weight of the transducer mount; (ii) uncertainty in the relative alignment between the sample mesh and the crystal axes; and (iii) uncertainty in the sample density. The first two of these each contribute a systematic uncertainty of approximately 1 GPa. The uncertainty in the density contributes an uncertainty of approximately 1%. We discuss these uncertainties in greater detail in the SM [28]. These systematic errors are general to RUS and not specific to the fitting methods implemented here.

Methods: Density functional theory calculations.—We used density-functional theory to produce estimates of the elastic moduli of UTe_2. This involved total energy calculations following the procedure of Ravindran *et al.* [32]. The full-potential linearized augmented plane wave method [33] calculations employed the generalized gradient approximation [34] for the exchange correlation, wave function, and potential energy cutoffs of 16 and 200 Ry, respectively, muffin-tin sphere radii of 1.35 Å, and an $8 \times 8 \times 8$ k-point mesh. Spin-orbit coupling was fully taken into account in the assumed nonmagnetic state. The elastic tensor was extracted from fits of the total energy variations around the experimental structure [35] to the energy-strain formula [32], including linear terms. The resulting moduli are given in Table III.

Methods: Pulse-echo ultrasound.—We also measured the compressional and shear moduli of UTe_2 using a traditional pulse-echo ultrasound technique as outlined in Theuss *et al.* [36]. The elastic moduli are calculated by measuring the time between two successive sound echoes and using the known sample length and density. The uncertainty resulting in this analysis is dominated by a 5% uncertainty in sample thickness.

Test results.—We test the implementation of two forward solvers—FEM and SMI—for fitting the RUS spectra of irregularly shaped samples using a genetic algorithm. We compare these results to the moduli extracted for rectangular parallelepiped samples that can be fit using the RPR forward solver, in addition to the FEM and SMI methods. We find agreement between all methods and all sample geometries to within our measurement uncertainties. It is worth noting that while both FEM and SMI are capable of fitting RUS spectra from irregularly shaped samples, the SMI method is two orders of magnitude faster than FEM, taking under an hour to produce a fit while FEM takes several days or even weeks.

$SrTiO_3$.—Our first test system for our new fitting method is $SrTiO_3$, whose elastic tensor consists of only three independent elements due to its cubic crystal structure (point group O_h). RUS measurements and fits are performed on two samples (Table I): Sample A was polished into a rectangular parallelepiped with dimensions $(1.49 \times 2.035 \times 3.02)$ mm^3, with edges oriented along the crystallographic axes. We can perform fits using all three methods—RPR, SMI, and FEM—in this simple geometry. Sample B was prepared with an irregular shape (see Fig. 1 for a 3D model based on a CT scan). Only SMI and FEM fits are possible for this geometry.

The fit results are given in Table I. We see that all methods yield identical results on the sample to within the given uncertainties. This demonstrates that, given the same experimental data and sample geometry, all three forward solvers implemented in a genetic algorithm yield the same elastic moduli. This is consistent with previous demonstrations that the three methods of forward computation—RPR, SMI, and FEM—are consistent to better than 1 part in 10^4 [26]. Note, however, that both RPR and SMI are roughly a factor of 100 faster than the FEM method (details on fit performance and parameters for all fits can be found in the SM [28]).

TABLE I. Elastic moduli of $SrTiO_3$ in GPa. The elastic moduli for both $SrTiO_3$ samples. The sample polished into the shape of a rectangular parallelepiped is sample A, and the irregularly shaped sample is sample B. The uncertainties are from a 2% increase in rms fit error. Additional systematic errors are estimated to be on the order of 1 GPa each (see SM [28]for more details). Literature values are provided for comparison.

Sample	Fit method	c_{11}	c_{12}	c_{44}
$SrTiO_3$ A	RPR	321.9 ±0.5	103.6 ±0.6	125.0 ±0.3
	FEM	321.9 ±0.5	103.6 ±0.6	125.0 ±0.3
	SMI	321.9 ±0.5	103.6 ±0.6	125.0 ±0.3
$SrTiO_3$ B	FEM	316.7 ±0.5	103.1 ±0.6	121.9 ±0.3
	SMI	316.7 ±0.5	102.9 ±0.6	122.0 ±0.3
Bell and Rupprecht [37]		317	102	123
Poindexter and Giardini [38]		348	101	119
Lüthi and Moran [39]		331	105	126
Migliori *et al.* [29]		315 ±0.6	102 ±0.7	122 ±0.01

We find differences of less than 2.5% for all elastic moduli when comparing the rectangular parallelepiped (sample A) and irregular (sample B) samples. These differences are slightly larger than our statistical uncertainties. These deviations could be due to deviations of sample A from a perfect rectangular parallelepiped. All of our results are compatible within uncertainty to the measurements of Bell and Rupprecht [37] and Migliori *et al.* [29] (bottom rows of Table I). Both Poindexter and Giardini [38] and Lüthi and Moran [39] report values for c_{11} that are nearly 10% larger than the value we obtain. While this deviation is significantly larger than our uncertainties, it is consistent with the 10% error in absolute elastic moduli measured with pulse-echo ultrasound (the technique used in [39]; see our pulse-echo measurements on UTe_2 in Table III as a reference).

We observe that both the elastic moduli and their uncertainties are identical between different samples and solver methods. They are also consistent with the uncertainties measured in Migliori *et al.* [29]. We therefore conclude that our new fitting methods provide reliable elastic moduli, even for samples with irregular geometries.

Mn_3Ge.—Next, we test hexagonal Mn_3Ge, point group D_{6h}, which has five independent elastic moduli. Fit results are given in Table II. Similar to $SrTiO_3$, we show fit results for a rectangular parallelepiped sample (sample A) with dimensions $(0.87 \times 1.01 \times 1.19)$ mm^3 and corners parallel to high-symmetry directions, as well as an irregularly shaped sample (sample B, see Fig. 1 for a 3D model).

As with $SrTiO_3$, all fit methods yield the same moduli for Mn_3Ge for both samples to within measurement uncertainty. Our results for sample A are also in agreement with previously published elastic moduli of Mn_3Ge [40]. Comparing samples A and B, the absolute difference in elastic moduli is below 4 GPa. This value is consistent with our results for $SrTiO_3$ and is likely due to similar systematic uncertainties described above. Again, there is no significant difference in the resulting moduli or their uncertainties for the different fit methods (see Table II).

Application to UTe_2.—Having successfully demonstrated the extraction of elastic moduli from RUS spectra for irregularly shaped samples, we now fit for the elastic moduli of two irregularly shaped, single-crystal samples of UTe_2. Three-dimensional models of both samples are shown in Fig. 1, and the moduli are given in Table III.

UTe_2 is orthorhombic (point group D_{2h}), with nine independent elastic moduli. The population size—the number of initial guesses—required for a good fit using a genetic algorithm scales roughly linearly with the number of free parameters [30]. This means that the UTe_2 fits require nearly twice the population as compared to the previous Mn_3Ge fits. Additionally, the samples of $SrTiO_3$ and Mn_3Ge were produced by adding additional facets to what were previously rectangular paraellelpiped samples, whereas our UTe_2 samples are as grown. This results in smaller feature sizes on the UTe_2 samples in comparison to the previous samples, requiring a finer mesh size for the 3D models (see SM [28] for details).

TABLE II. Elastic moduli of Mn_3Ge in GPa. The elastic moduli for both Mn_3Ge samples. A rectangular parallelepiped is sample A, and the irregularly shaped sample is sample B. The uncertainties are from a 2% increase in rms fit error. Additional systematic errors are estimated to be on the order of 1 GPa each (see SM [28] for more details).

Sample	Fit method	c_{11}	c_{12}	c_{13}	c_{33}	c_{44}
Mn_3Ge A	RPR	130.0	43.9	13	202	48.3
		±0.3	±0.4	±2	±2	±0.2
	FEM	130.0	43.9	13	202	48.3
		±0.3	±0.3	±2	±2	±0.2
	SMI	130.0	43.9	13	202	48.3
		±0.3	±0.4	±2	±2	±0.2
Mn_3Ge B	FEM	126.8	40.3	14	203	48.7
		±0.3	±0.4	±4	±2	±0.2
	SMI	126.8	40.2	14	203	48.7
		±0.3	±0.4	±4	±2	±0.2

Both the dense mesh of our particular sample, and large number of moduli for UTe_2 in general, increase the fit time for the FEM method, which must recompute the entire spectrum at each stage of the fit. This makes FEM unsuitable for fitting elastic moduli, as convergence would take upward of a month. The SMI method, on the other hand, is largely unaffected by the increase in population size and mesh density because the computationally intensive step is performed only once, at the start of the fit, and the results are stored for use in subsequent generations of the genetic algorithm. We therefore only perform SMI fits to our UTe_2 spectra. This approach is justified by the results of the previous section, which demonstrated that fits using both FEM and SMI methods produce identical elastic moduli.

We find excellent agreement between the elastic moduli of UTe_2 samples A and B at both 300 K and 4 K (see Table III). For additional comparison, we present elastic moduli measured with pulse-echo ultrasound. We find no significant difference between these values and the ones obtained using RUS and we note that the uncertainties are greatly reduced using RUS. Also note that obtaining c_{12}, c_{13}, and c_{23} from pulse echo would require three additional experiments performed in different directions. We also report elastic moduli obtained from density-functional theory calculations (bottom row in Table III). These calculated values are in remarkable agreement with the experimental results. Other experimentally relevant quantities, including the bulk modulus, the Young's moduli, and the Poisson's ratios, are tabulated in the SM [28].

Conclusion.—We implement two methods for performing the forward calculation for resonance spectra into a genetic algorithm. These methods—SMI and FEM—allow

TABLE III. Elastic moduli of UTe_2 in GPa. The elastic moduli of UTe_2 samples A and B, shown in Fig. 1, at 300 K and at 4 K. The uncertainties are from a 2% increase in rms fit error. Additional systematic errors are estimated to be on the order of 1 GPa each (see SM [28] for more details). Also shown are the elastic moduli obtained with conventional pulse-echo ultrasound measurements, with uncertainties caused mainly by the uncertainty of the sample dimensions. Moduli obtained from DFT calculations, with atomic coordinates optimized, are given on the bottom row. The DFT values were used as rough guides to constrain the parameter space of the genetic algorithm fits to the RUS data.

	T (K)	c_{11}	c_{22}	c_{33}	c_{12}	c_{13}	c_{23}	c_{44}	c_{55}	c_{66}
UTe_2 A	4	90.3 ±0.2	144.1 ±0.6	95.9 ±0.2	25.7 ±0.8	41.3 ±0.2	31.9 ±0.5	28.05 ±0.08	53.2 ±0.2	30.43 ±0.08
	300	84.7 ±0.2	139.5 ±0.5	91.1 ±0.2	26.8 ±0.6	38.1 ±0.2	31.6 ±0.5	26.93 ±0.07	52.4 ±0.2	29.65 ±0.08
UTe_2 B	4	89.2 ±0.3	146.9 ±0.9	94.0 ±0.3	28 ±1	40.4 ±0.2	31.4 ±0.9	28.2 ±0.1	52.5 ±0.3	30.3 ±0.1
	300	82.8 ±0.3	141.8 ±0.8	89.9 ±0.3	26 ±1	36.7 ±0.2	32.7 ±0.7	27.18 ±0.09	51.5 ±0.3	29.0 ±0.1
Pulse Echo	280	81 ±8	141 ±15	91 ±11	⋯ ⋯	⋯ ⋯	⋯ ⋯	27 ±3	52 ±5	30 ±3
DFT		96	136	90	28	46	26	28	57	31

us to fit the elastic moduli of irregularly shaped samples using resonant ultrasound spectroscopy data. This is first demonstrated on materials with known elastic moduli ($SrTiO_3$ and Mn_3Ge), establishing consistency between our new methods and the older method of Visscher *et al.* [22], which is only applicable for regularly shaped samples. Our method is 100 times faster than an equivalent implementation using finite elements methods as the forward solver (see the SM [28] for timing details). We then apply our new method to measure the full elastic tensor of the unconventional superconductor UTe_2 at 300 K and at 4 K (Table III).

We expect that the elastic moduli of UTe_2 will be of use to researchers studying the superconducting properties under both uniaxial strain and hydrostatic pressure [9,10,15,17,18,41]. We expect that the general method that we have introduced—implementing the fast surface mesh integration method into a genetic algorithm—will be broadly useful for measuring the elastic moduli of samples that cannot be easily prepared into regular geometric shapes.

The code used to fit resonant ultrasound spectroscopy spectra is publicly available on GitHub [42].

B. J., F. T., G. G., and A. S. acknowledge funding from the Office of Basic Energy Sciences of the United States Department of Energy under Award No. DE-SC0020143 (UTe_2 and $SrTiO_3$ sample preparation, ultrasound experiments, and data analysis). B. J. R., F. T., G. G., A. S., T. C., and S. N. acknowledge funding from the Institute for Quantum Matter, an Energy Frontier Research Center funded by the Office of Basic Energy Sciences of the United States Department of Energy under Award No. DE-SC0019331 (Mn_3Ge sample growth and preparation). Imaging data was acquired through the Cornell Institute of Biotechnology's Imaging Facility, with NIH S10OD012287 for the ZEISS/Xradia Versa 520 X-ray Microscope (CT). Laue backreflection diffraction measurements made use of the Cornell Center for Materials Research Shared Facilities which are supported through the NSF MRSEC program (DMR-1719875). Research at the University of Maryland was supported by the Department of Energy under Award No. DE-SC-0019154 (sample characterization), the Gordon and Betty Moore Foundation's EPiQS Initiative through Grant No. GBMF9071 (materials synthesis), NIST, and the Maryland Quantum Materials Center. Discussion of commercial software does not imply endorsement by NIST.

*bradramshaw@cornell.edu

[1] S. Ran, C. Eckberg, Q.-P. Ding, Y. Furukawa, T. Metz, S. R. Saha, I.-L. Liu, M. Zic, H. Kim, J. Paglione, and N. P. Butch, Nearly ferromagnetic spin-triplet superconductivity, Science **365**, 684 (2019).

[2] D. Aoki, A. Nakamura, F. Honda, D. Li, Y. Homma, Y. Shimizu, Y. J. Sato, G. Knebel, J.-P. Brison, A. Pourret, D. Braithwaite, G. Lapertot, Q. Niu, M. Vališka, H. Harima, and J. Flouquet, Unconventional superconductivity in heavy fermion UTe_2, J. Phys. Soc. Jpn. **88**, 043702 (2019).

[3] S. Ran, S. R. Saha, I.-L. Liu, D. Graf, J. Paglione, and N. P. Butch, Expansion of the high field-boosted superconductivity in UTe_2 under pressure, npj Quantum Mater. **6**, 1 (2021).

[4] G. Nakamine, S. Kitagawa, K. Ishida, Y. Tokunaga, H. Sakai, S. Kambe, A. Nakamura, Y. Shimizu, Y. Homma, D. Li, F. Honda, and D. Aoki, Superconducting properties of

heavy fermion UTe_2 revealed by ^{125}Te-nuclear magnetic resonance, J. Phys. Soc. Jpn. **88**, 113703 (2019).
[5] G. Nakamine, K. Kinjo, S. Kitagawa, K. Ishida, Y. Tokunaga, H. Sakai, S. Kambe, A. Nakamura, Y. Shimizu, Y. Homma, D. Li, F. Honda, and D. Aoki, Inhomogeneous superconducting state probed by ^{125}Te NMR on UTe_2, J. Phys. Soc. Jpn. **90**, 064709 (2021).
[6] H. Fujibayashi, G. Nakamine, K. Kinjo, S. Kitagawa, K. Ishida, Y. Tokunaga, H. Sakai, S. Kambe, A. Nakamura, Y. Shimizu, Y. Homma, D. Li, F. Honda, and D. Aoki, Superconducting order parameter in UTe_2 determined by knight shift measurement, J. Phys. Soc. Jpn. **91**, 043705 (2022).
[7] G. Knebel, W. Knafo, A. Pourret, Q. Niu, M. Vališka, D. Braithwaite, G. Lapertot, M. Nardone, A. Zitouni, S. Mishra, I. Sheikin, G. Seyfarth, J. P. Brison, D. Aoki, and J. Flouquet, Field-reentrant superconductivity close to a metamagnetic transition in the heavy-fermion superconductor UTe_2, J. Phys. Soc. Jpn. **88**, 063707 (2019).
[8] S. Ran, I. L. Liu, Y. S. Eo, D. J. Campbell, P. M. Neves, W. T. Fuhrman, S. R. Saha, C. Eckberg, H. Kim, D. Graf, F. Balakirev, J. Singleton, J. Paglione, and N. P. Butch, Extreme magnetic field-boosted superconductivity, Nat. Phys. **15**, 1250 (2019).
[9] S. Ran, H. Kim, I.-L. Liu, S. R. Saha, I. Hayes, T. Metz, Y. S. Eo, J. Paglione, and N. P. Butch, Enhancement and reentrance of spin triplet superconductivity in UTe_2 under pressure, Phys. Rev. B **101**, 140503 (2020).
[10] D. Aoki, F. Honda, G. Knebel, D. Braithwaite, A. Nakamura, D. X. Li, Y. Homma, Y. Shimizu, Y. J. Sato, J. P. Brison, and J. Flouquet, Multiple superconducting phases and unusual enhancement of the upper critical field in UTe_2, J. Phys. Soc. Jpn. **89**, 053705 (2020).
[11] D. S. Wei, D. Saykin, O. Y. Miller, S. Ran, S. R. Saha, D. F. Agterberg, J. Schmalian, N. P. Butch, J. Paglione, and A. Kapitulnik, Interplay between magnetism and superconductivity in UTe_2, Phys. Rev. B **105**, 024521 (2022).
[12] I. M. Hayes, D. S. Wei, T. Metz, J. Zhang, Y. S. Eo, S. Ran, S. R. Saha, J. Collini, N. P. Butch, D. F. Agterberg, A. Kapitulnik, and J. Paglione, Multicomponent superconducting order parameter in UTe_2, Science **373**, 797 (2021).
[13] A. Rosuel, C. Marcenat, G. Knebel, T. Klein, A. Pourret, N. Marquardt, Q. Niu, S. Rousseau, A. Demuer, G. Seyfarth, G. Lapertot, D. Aoki, D. Braithwaite, J. Flouquet, and J.-P. Brison, Field-induced tuning of the pairing state in a superconductor, arXiv:2205.04524.
[14] L. P. Cairns, C. R. Stevens, C. D. O'Neill, and A. Huxley, Composition dependence of the superconducting properties of UTe_2, J. Phys. Condens. Matter **32**, 415602 (2020).
[15] S. M. Thomas, C. Stevens, F. B. Santos, S. S. Fender, E. D. Bauer, F. Ronning, J. D. Thompson, A. Huxley, and P. F. S. Rosa, Spatially inhomogeneous superconductivity in UTe_2, Phys. Rev. B **104**, 224501 (2021).
[16] P. F. S. Rosa, A. Weiland, S. S. Fender, B. L. Scott, F. Ronning, J. D. Thompson, E. D. Bauer, and S. M. Thomas, Single thermodynamic transition at 2 K in superconducting UTe_2 single crystals, Commun. Mater. **3**, 33 (2022).
[17] D. Braithwaite, M. Vališka, G. Knebel, G. Lapertot, J.-P. Brison, A. Pourret, M. E. Zhitomirsky, J. Flouquet, F. Honda, and D. Aoki, Multiple superconducting phases in a nearly ferromagnetic system, Commun. Phys. **2**, 147 (2019).
[18] C. Girod, C. R. Stevens, A. Huxley, E. D. Bauer, F. B. Santos, J. D. Thompson, R. M. Fernandes, J.-X. Zhu, F. Ronning, P. F. S. Rosa, and S. M. Thomas, Thermodynamic and electrical transport properties of UTe_2 under uniaxial stress, Phys. Rev. B **106**, L121101 (2022).
[19] M. E. Barber, F. Lechermann, S. V. Streltsov, S. L. Skornyakov, S. Ghosh, B. Ramshaw, N. Kikugawa, D. A. Sokolov, A. P. Mackenzie, C. W. Hicks *et al.*, Role of correlations in determining the Van Hove strain in Sr_2RuO_4, Phys. Rev. B **100**, 245139 (2019).
[20] Y.-S. Li, M. Garst, J. Schmalian, S. Ghosh, N. Kikugawa, D. A. Sokolov, C. W. Hicks, F. Jerzembeck, M. S. Ikeda, Z. Hu, B. J. Ramshaw, A. W. Rost, M. Nicklas, and A. P. Mackenzie, Elastocaloric determination of the phase diagram of Sr_2RuO_4, Nature (London) **607**, 276 (2022).
[21] M. D. Bachmann *et al.*, Spatial control of heavy-fermion superconductivity in $CeIrIn_5$, Science **366**, 221 (2019).
[22] W. M. Visscher, A. Migliori, T. M. Bell, and R. A. Reinert, On the normal modes of free vibration of inhomogeneous and anisotropic elastic objects, J. Acoust. Soc. Am. **90**, 2154 (1991).
[23] G. Liu and J. Maynard, Measuring elastic constants of arbitrarily shaped samples using resonant ultrasound spectroscopy, J. Acoust. Soc. Am. **131**, 2068 (2012).
[24] J. Plesek, R. Kolman, and M. Landa, Using finite element method for the determination of elastic moduli by resonant ultrasound spectroscopy, J. Acoust. Soc. Am. **116**, 282 (2004).
[25] B. J. Ramshaw, A. Shekhter, R. D. McDonald, J. B. Betts, J. N. Mitchell, P. H. Tobash, C. H. Mielke, E. D. Bauer, and A. Migliori, Avoided valence transition in a plutonium superconductor, Proc. Natl. Acad. Sci. U.S.A. **112**, 3285 (2015).
[26] A. Shragai, F. Theuss, G. Grissonnanche, and B. J. Ramshaw, Rapid method for computing the mechanical resonances of irregular objects, J. Acoust. Soc. Am. **153**, 119 (2023).
[27] F. F. Balakirev, S. M. Ennaceur, R. J. Migliori, B. Maiorov, and A. Migliori, Resonant ultrasound spectroscopy: The essential toolbox, Rev. Sci. Instrum. **90**, 121401 (2019).
[28] See Supplemental Material at http://link.aps.org/supplemental/10.1103/PhysRevLett.132.066003 for all measured experimental resonance spectra, a detailed uncertainty analysis of our fits, and sample digitization details. We also tabulate values of bulk moduli, Young's moduli, and Poisson's ratios, as well as compare convergence times for the different forward solver methods. The supplement includes Refs. [18,22,25–27,29–31].
[29] A. Migliori, J. L. Sarrao, W. M. Visscher, T. M. Bell, M. Lei, Z. Fisk, and R. G. Leisure, Resonant ultrasound spectroscopic techniques for measurement of the elastic moduli of solids, Physica (Amsterdam) **183B**, 1 (1993).
[30] R. Storn and K. Price, Differential evolution: A simple and efficient heuristic for global optimization over continuous spaces, J. Global Optim. **11**, 341 (1997).
[31] P. Virtanen *et al.* (SciPy1.0 Contributors), SciP1.0: Fundamental algorithms for scientific computing in PYTHON, Nat. Methods **17**, 261 (2020).

[32] P. Ravindran, L. Fast, P. A. Korzhavyi, B. Johansson, J. Wills, and O. Eriksson, Density functional theory for calculation of elastic properties of orthorhombic crystals: Application to $TiSi_2$, J. Appl. Phys. **84**, 4891 (1998).
[33] M. Weinert, G. Schneider, R. Podloucky, and J. Redinger, FLAPW: Applications and implementations, J. Phys. Condens. Matter **21**, 084201 (2009).
[34] J. P. Perdew, K. Burke, and M. Ernzerhof, Generalized gradient approximation made simple, Phys. Rev. Lett. **77**, 3865 (1996).
[35] S. Ikeda, H. Sakai, D. Aoki, Y. Homma, E. Yamamoto, A. Nakamura, Y. Shiokawa, Y. Haga, and Y. Ōnuki, Single crystal growth and magnetic properties of UTe_2, J. Phys. Soc. Jpn. **75**, 116 (2006).
[36] F. Theuss, A. Shragai, G. Grissonnanche, I. M. Hayes, S. R. Saha, Y. S. Eo, A. Suarez, T. Shishidou, N. P. Butch, J. Paglione, and B. J. Ramshaw, Single-component superconductivity in UTe_2 at ambient pressure, arXiv:2307.10938.
[37] R. O. Bell and G. Rupprecht, Elastic constants of strontium titanate, Phys. Rev. **129**, 90 (1963).
[38] E. Poindexter and A. A. Giardini, Elastic constants of strontium titanate ($SrTiO_3$), Phys. Rev. **110**, 1069 (1958).
[39] B. Lüthi and T. J. Moran, Sound propagation near the structural phase transition in strontium titanate, Phys. Rev. B **2**, 1211 (1970).
[40] F. Theuss, S. Ghosh, T. Chen, O. Tchernyshyov, S. Nakatsuji, and B. J. Ramshaw, Strong magnetoelastic coupling in Mn_3X (X = Ge, Sn), Phys. Rev. B **105**, 174430 (2022).
[41] S. M. Thomas, F. B. Santos, M. H. Christensen, T. Asaba, F. Ronning, J. D. Thompson, E. D. Bauer, R. M. Fernandes, G. Fabbris, and P. F. S. Rosa, Evidence for a pressure-induced antiferromagnetic quantum critical point in intermediate-valence UTe_2, Sci. Adv. **6**, eabc8709 (2020).
[42] https://github.com/CHiLL-Ramshaw/rus_fitting.

Correction: Missing information from the first sentence of the Acknowledgments has been inserted. The omission of a support statement has also been fixed.